Structural Theory for Non-stoicheiometry. Part I. Defect Fluorite-type Structures: Lanthanoid Oxides MO_x with $1{\cdot}7 \leqslant x \leqslant 2{\cdot}0$

By **Raymond L. Martin,** Research School of Chemistry, Australian National University, P.O. Box No. 4, Canberra, Australia 2600

The concept of an octahedrally co-ordinated anion vacancy $\square O_6$ is introduced to develop a rational structural theory for the known series of ordered non-stoicheiometric lanthanoid oxides of formula M_nO_{2n-2} (n = 7—∞). The resulting co-ordination defect (c.d.) has the composition $M_{\frac{2}{3}}\square O_6$ and it is suggested that this retains its structural integrity in all the homologues. Topological analysis has been employed to establish the fundamental superstructures of the fluorite lattice which characterize these oxide phases. It emerges that the anion deficiency is accommodated by point defects gathered in oblique {213} planes each being separated by (n − 1) oxide-intact {213} planes. Effectively, all these phases are based on regularly spaced intergrowths of the progenitors ι-Pr_7O_{12} and PrO_2. It is shown that the homologues are structurally coherent and that irregularity in spacing of intergrown phases provides a logical description for the grossly non-stoicheiometric α-phase which overlays the region $MO_{1\cdot7}$—$MO_{2\cdot0}$ at higher temperatures. The extended {213} sheets of defects can be circumscribed coherently by PrO_2 to generate finite discs of $Pr_{\frac{2}{3}}\square O_6$. Order–disorder transformations are considered in terms of the interchangeability of $Pr_{\frac{2}{3}}\square O_6$ and $Pr_{\frac{2}{3}}O_7$ structural sub-units which are topologically identical. The non-existence of the homologue Pr_8O_{14} and a possible structure for the β′-$Pr_{12}O_{22}$ phase are examined in terms of the cubic pyrochlore ($E8_1$) structure.

BINARY oxides of transition, lanthanoid, and actinoid elements are frequently characterized at higher temperatures by non-stoicheiometric phases of extended compositional width. Prolonged annealing at lower temperatures generally permits such phases to be resolved into a succession of discrete, ordered, intermediate compounds with well defined compositions and interrelated by some common structural principle. In a few cases the crystal structure of an ordered phase is known so that the ideal composition can be determined from the numbers of each type of atom in the unit cell. Since the symmetry is frequently lower and the volume larger than the parent structure, the derived formula is often cumbersome. Nevertheless, it must reflect the manner in which the deviation from ideal stoicheiometry is being accommodated in the lattice.

Structural relations so far established between ordered phases of binary oxides and chalcogenides of the transition metals have exposed the limitations of classical concepts of non-stoicheiometry in which irrational formulae were formerly ascribed to random distributions of point defects (*i.e.* vacancies or interstitial atoms) in the host lattice. The pioneering crystallographic work of A. Magneli,[1] A. D. Wadsley and S. Andersson,[2] and others [3] has forced a reappraisal of this traditional viewpoint and led to recognition of the fundamental structural concept of crystallographic shear. Recent application of more incisive techniques such as electron microscopy and electron diffraction has introduced a new dimension of perception into the mechanistic and topological role of crystallographic shear in defining structural relations within a variety of ' Magneli phases ' of general formulae M_nO_{3n-1} and M_nO_{3n-2} derived from the ReO_3 structure and M_nO_{2n-1} derived from the TiO_2 structure.[4]

Although the chemistry of certain lanthanoid oxides is also characterized by apparently similar formal relations between disordered and well defined ordered phases of composition M_nO_{2n-2}, the structural principles by which they are interrelated must differ and, at present, are imperfectly resolved.[5] Crystallographic shear has been specifically excluded [5] due to the absence of short M–M distances in fluorite-based MO_x structures. A viable alternative requires that point defects are ordered to give superstructures of the MO_2 fluorite lattice ($C1$ structure), derived in concept either by incorporating oxygen atoms into vacant sites of the type-C sesquioxide M_2O_3($D5_3$ structure), or by creating anion vacancies in the perfect $C1$ structure. The unsolved problem of central significance is to identify the origin of short- and long-range forces which regulate the ordering process and determine the nature of the ensuing superstructures.

In binary and ternary oxides of this type, X-ray

[1] A. Magnéli, ' The Chemistry of Extended Defects in Non-metallic Solids,' eds. L. Eyring and M. O'Keeffe, North-Holland, Amsterdam, 1970, p. 148.

[2] A. D. Wadsley and S. Andersson, ' Perspectives in Structural Chemistry,' eds. J. D. Dunitz and J. A. Ibers, John Wiley, 1970, vol. VIII, p. 1.

[3] See, for example, D. J. M. Bevan, ' Comprehensive Inorganic Chemistry,' Pergamon, Oxford, 1973, vol. 4, p. 453.

[4] J. G. Allpress, J. V. Sanders, and A. D. Wadsley, *Acta Cryst.*, 1969, **B25**, 1156.

[5] B. G. Hyde, D. J. M. Bevan, and L. Eyring, *Phil. Trans. Roy. Soc.* (*London*), 1966, **A259**, 583.

and density measurements have established that the cation lattice remains intact for all compositions between M_2O_3 and MO_2. It is consequential that on oxidation the co-ordination number of the metal ion must increase. Thus, in principle, the $D5_3$ structure can be derived from the $C1$ structure by ordered omission of oxygen atoms along the four $\langle 111\rangle_{cub.}$ directions of cubic MO_2 so that the co-ordination polyhedra are transformed progressively from MO_8 to MO_6. An intermediate phase of composition M_7O_{12} is known to possess a rhombohedral primitive cell which is a supercell of the M_7O_{14} parent.[6] It has been established that all oxygen sites which lie along the unique three-fold $[111]_{cub.}$ axis [Figure 1(*a*)] are vacant so that cations situated on this axis (1/7) are six-co-ordinated with their near-neighbours (6/7) being seven-co-ordinate [7] [Figure 1(*b*)].

Hyde *et al.*[8] have proposed that the linear infinite MO_6 'string' [*cf.* Figure 1(*b*)], surrounded by a contiguous 'sheath' of MO_7, is the structural entity which generates the series M_nO_{2n-2} from the parent MO_2. If $1/n$ of the cations are located in the 'strings,' the composition of the ordered phases becomes $MO_{2[1-(1/n)]}$ or M_nO_{2n-2}. The 'string' may be regarded as the '*extended defect*' in the *f* transition-metal oxides analogous to the Wadsley '*shear defect*' in *d* transition-metal oxides.[3] Thornber *et al.*[9] have subsequently suggested that the 'string' proposal is not entirely correct noting that such 'strings' are absent in the structure of the pseudo-binary $Zr_5Sc_2O_{13}$ (*i.e.* $n = 14$). However, the principal difference between extended defects in $Zr_3Sc_4O_{12}$ and in $Zr_{10}Sc_4O_{26}$ [*cf.* Figure 1(*c*)] arises because one half of the anion vacancies along the three-fold axis have been annihilated in a pairwise fashion concomitant with addition of $7ZrO_2$ to form the latter phase. As a consequence metal atoms lying along this axis become alternately six- and eight-co-ordinate rather than simply six-co-ordinate as in the parent M_7O_{12} structure. These authors have extended the Sawyer *et al.* concept [7] of a defect cluster of six seven-co-ordinate cations about one six-co-ordinate cation ($M_7O_{36}\square_2$) to describe these phases. They propose that the basic structural principle for all M_nO_{2n-2} phases is the ordered space-filling arrangement of edge-sharing M_7O_{36} and M_7O_{38} sub-units to yield coherent microdomains of M_7O_{12} and MO_2, a concept which can be readily extended to grossly non-stoicheiometric phases observed at higher temperatures. In their view, the 'strings' described earlier result simply from stacking of fully edge-shared M_7O_{36} units, all being oriented parallel to the unique three-fold axis.

In contrast, Caro [10,11] has directed attention to packing of oxygen- rather than metal-centred co-ordination polyhedra as an alternative and useful representation of the lanthanoid oxides. Relations between hexagonal (type A), monoclinic (type B), and cubic (type C) forms of the sesquioxides M_2O_3 were successfully examined, from which the concept of a complex 'lanthanyl' cationic structural unit $(MO)_n^{n+}$ arose. Caro suggested that the homologous series of ordered lanthanoid oxides can be described by interweaving slabs of $(MO)_n^{n+}$ ions with layers of defect fluorite MO_2 in which one sixth of the anions are missing in each oxygen plane. Effectively, {111} sheets of edge-sharing M_4O or $M_4\square$ tetrahedra are stacked in some repeating pattern to accommodate the non-stoicheiometry. Significantly, Caro concludes that the accepted classical formula M_nO_{2n-2} must be in error because limiting compositions of his {111} sheets are $(MO)_n^{n+}$ and M_6O_{10} and so lead to the composition $M_{6n+3}O_{11n+5}$ for the homologous series.

Whilst these models provide an overall structural formalism for accommodating oxygen deficiency in a rational manner, they do not identify the origin of the underlying short- and long-range forces nor provide detailed insight into geometric dispositions of anion vacancies in superstructures which must characterize each of the ordered homologues. Furthermore, the structural mechanism by which the ordered phases are generated, which could illuminate transport processes in defect oxides, remains unknown.

Unfortunately, the desired characterization of each homologue by single-crystal diffraction methods is rendered difficult by the extraordinary ease with which oxygen can be transferred between the MO_x lattice and the oxygen environs.[5,12] As a result, synthesis of well ordered crystals is inherently difficult due to the remarkably high oxygen mobility which inhibits quenching-in of both composition and order in samples equilibrated even at moderate temperatures. However, *X*-ray powder-diffraction measurements do support the view that M_nO_{2n-2} homologues are probably highly ordered superstructures of low symmetry derived from the MO_2 parent.[7] Unfortunately, intensities of Bragg reflections cannot furnish direct evidence on the nature of the defects present, although a measure of fractional occupancy of an atom in a given site is provided. As the complexity of the structure and dimensions of the unit cell increase, the problem is aggravated and even single-crystal studies can be of limited value.[2] In these circumstances, the need for a theory with which the probable structures can be predicted becomes particularly pressing.

I describe here an attempt to formulate such a theory based on the premise that lanthanoid oxides are good approximations to the perfect ionic lattice. It follows

[6] N. C. Baenziger, H. A. Eick, H. S. Schuldt, and L. Eyring, *J. Amer. Chem. Soc.*, 1961, **83**, 2219.

[7] J. O. Sawyer, B. G. Hyde, and L. Eyring, *Bull. Soc. chim. France*, 1965, 1190.

[8] B. G. Hyde, D. J. M. Bevan, and L. Eyring, *Internat. Conf. Electron Diffraction and Crystal Defects*, Austral. Acad. Sci., 1965, paper 11, C-4.

[9] M. R. Thornber, D. J. M. Bevan, and J. Graham, *Acta Cryst.*, 1968, **B24**, 1183.

[10] P. E. Caro, *Proc. 5th Materials Research Symp. 'Solid State Chemistry,'* NBS Spec. Publ., 364, 1972, pp. 367—383.

[11] P. E. Caro, *J. Solid-state Chem.*, 1973, **6**, 396.

[12] J. S. Anderson and R. L. Martin, unpublished work; R. L. Martin, 'A Study of the Oxides of Praseodymium,' M.Sc. Thesis, University of Melbourne, 1948.

that the origin of the forces which determine short- and long-range ordering of oxygen vacancies in a sensibly perfect metal sub-lattice is likewise predominantly electrostatic. The consequences which derive from this basic assumption are explored below and it will be shown that probable structures for all the observed low- and high-temperature phases of binary lanthanoid oxides in the range $MO_{1\cdot7}$—$MO_{2\cdot0}$ emerge naturally. Some of their more pertinent characteristics which require explanation are first summarized.

RESULTS AND DISCUSSION

Homology of Ce, Pr, *and* Tb *Oxides.*—Binary lanthanoid oxide–oxygen systems, $MO_x + O_2$ (M = Ce, Pr, or Tb; $1\cdot5 \leqslant x \leqslant 2\cdot0$) provide pre-eminent examples of non-stoicheiometric phases based on the fluorite *C*1 structure.

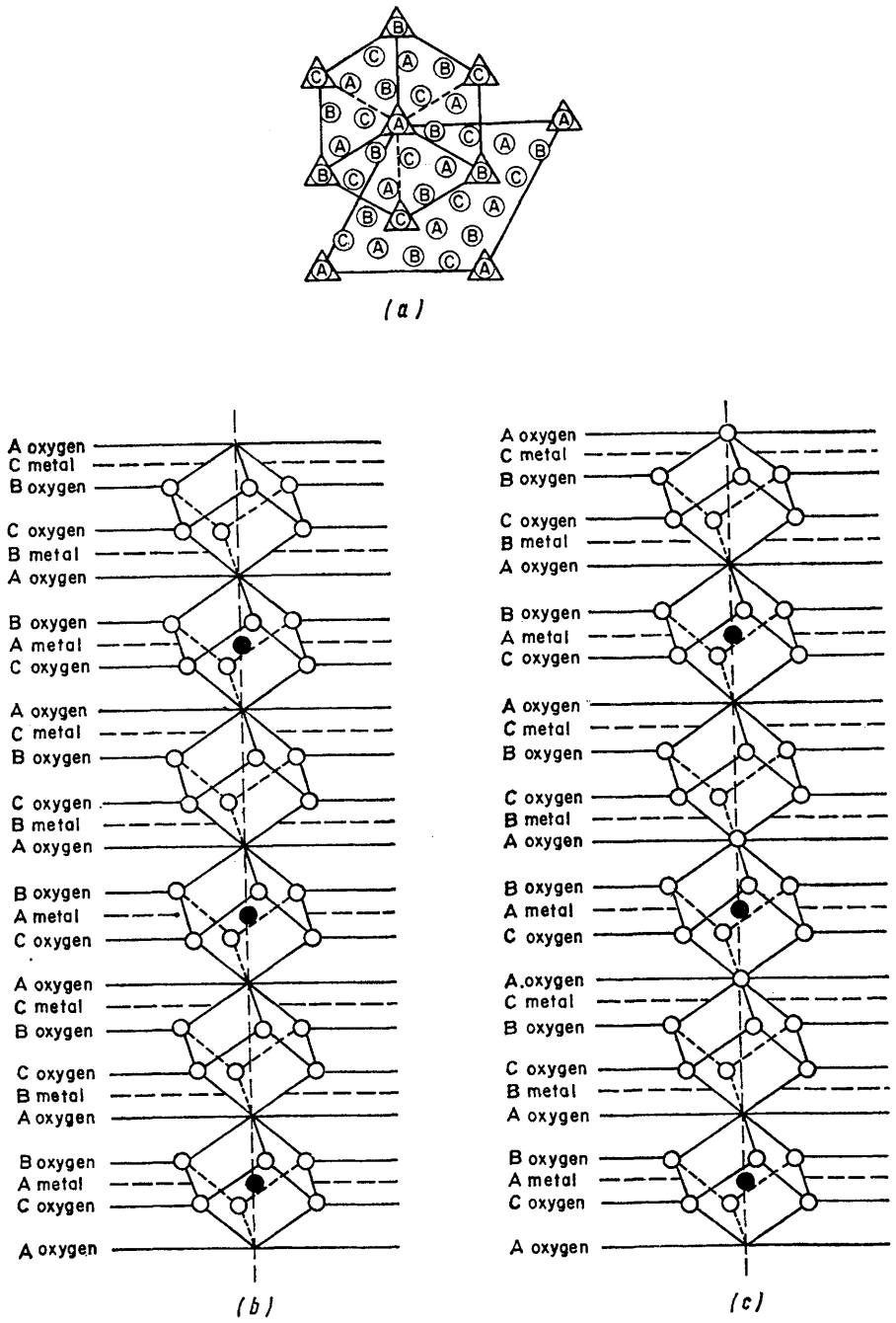

FIGURE 1 (*a*) Projection of atom positions on the (001) hexagonal plane for the *C*1 structure. The unit cell shown is common to the ideal structures of both $Zr_3Sc_4O_{12}$ and $Zr_{10}Sc_4O_{26}$; (*b*) linear infinite 'string' characteristic of the M_7O_{12} structure. Stacking sequence of metal and oxygen layers in the vicinity of a three-fold rotation axis chosen to pass through atoms in the A layers of the cubic close-packed sequence; (*c*) modified 'string' found in $Zr_{10}Sc_4O_{26}$

It is these elements with electron configurations $4f^15d^16s^2$, $4f^36s^2$, and $4f^96s^2$ that display both III and IV oxidation states. Since $4f$ orbitals are compact radially, their oxides are essentially ionic. Directional forces due to metal–ligand overlap should not be a factor which influences the order of anion vacancies or the stereochemistry of metal–oxygen polyhedra. For praseodymium, extensive tensimetric, isobaric, and *X*-ray studies have established [5] the succession of discrete ordered phases with the narrow range of homogeneity summarized in Table 1. Members of the homologous

TABLE 1

Stoicheiometry of homologous phases, Pr_nO_{2n-2}

		x in PrO_x		
n	Formula	Calc.	Expt.[a]	Phase symbol
4	Pr_4O_6	1·500	1·500	θ ($D5_2$ or type A) ϕ ($D5_3$ or type C)
7	Pr_7O_{12}	1·714	1·713—1·719	ι
8	Pr_8O_{14}	1·750		
9	Pr_9O_{16}	1·778	1·776—1·778	ζ
10	$Pr_{10}O_{18}$	1·800	1·799—1·801	ε
11	$Pr_{11}O_{20}$	1·818	1·817—1·820	δ
12	$Pr_{12}O_{22}$	1·833	1·831—1·836	β
14	$Pr_{14}O_{26}$	1·857		
∞	PrO_2	2·000	2·000	α

[a] Ref. 5.

series of stoicheiometric phases M_nO_{2n-2} ($n = 4$ and 7—∞) are also found in a number of other binary and ternary systems. However, information is most extensive for M = Pr and the present analysis will be concerned primarily with the binary praseodymium oxide–oxygen system even though crystallographic data are limited.

Each intermediate Pr_nO_{2n-2} phase decomposes peritectoidally (*i.e.* at successively higher temperatures as n decreases) to form a homologue of lower n and a disordered non-stoicheiometric face-centred-cubic (f.c.c.) phase (designated β′) of approximate composition $PrO_{1·83}$.[5] It is noteworthy that ι-Pr_7O_{12} is the terminal member, and it alone dissociates into a mixture of two disordered non-stoicheiometric phases, namely, the f.c.c. α-phase [13] for which $1·7 \lesssim x \lesssim 2·0$ and the body-centred-cubic (b.c.c.) phase [5] (designated σ) for which $1·7 > x \gtrsim 1·6$. Although both the α- and σ-phases have been traditionally regarded as being disordered structures derived from fluorite, it is highly significant that they are immiscible to a temperature [5] of 1 076 °C (*cf.* 1 169 °C in $CeO_x + O_2$ [14]). Immiscibility between cubic oxide phases was first established [12,15] in the closely analogous ternary system $Y_2O_3 + CeO_2 + O_2$ and no reliably authenticated example of miscibility has since emerged. That the miscibility gap is extremely narrow for praseodymium, *e.g.* $PrO_{1·695}$ to $PrO_{1·725}$, and that it should persist to such high temperatures without closing or even narrowing, indicates that a radical and persistent structural difference between the cubic σ- and α-phases must obtain.

More recently it has been suggested [16] that the α-phase which overlays the region $1·785 \lesssim x \lesssim 1·830$ exhibits a texture which can be resolved into four subregions occurring in the following ranges of oxygen pressure: α_1, 40—150; α_2, 170—220; α_3, 250—370; and α_4, 420—730 Torr. The low-temperature homologue which is the immediate precursor of the α-phase during an isobaric heating experiment, appears to be different in each of these regions. Thus ε-$PrO_{1·800} \rightarrow \alpha_1$, δ-$PrO_{1·818} \rightarrow \alpha_2$, β-$PrO_{1·833} \rightarrow \alpha_3$, and $PrO_{2·000} \rightarrow \alpha_4$, which suggests that the α-phase possesses a microdomain texture which is influenced in some way by the structure of the homologue from which it originated.

The existence of an M_8O_{14} phase is doubtful. This composition was originally assigned to air-ignited praseodymia,[17] but has been discounted by many subsequent investigations. Recent isobaric measurements with the TbO_x system provide tenuous evidence for the existence of the Tb_8O_{14} homologue at low oxygen pressures.[18] If a lacuna is genuinely present in the M_nO_{2n-2} series at $n = 8$, it might provide a sensitive criterion for evaluating competing structural theories.

Tensimetric [12,19] and isobaric [5] studies have established that the praseodymium oxide–oxygen system is remarkably dynamic. At temperatures as low as 400 °C, oxygen is still transported between the solid and gas phases with great facility. Even so, ' classically univariant ' diphasic regions of the phase diagram frequently exhibit hysteresis.[5,12,19] It has been established that there is no change in surface area accompanying oxidation and reduction of PrO_x phases,[20] which points towards a high degree of coherence between the ordered and disordered phases. However, even a small degree of mismatching will lead inevitably to lattice strain and induce hysteresis in phase transformations.[21] These characteristics require that close structural relations should persist between reactant and product in oxidative- and reductive-phase transformations and must be satisfactorily reproduced for any structural model to be convincing.

Structural Model: Role of the Co-ordination Defect.— Since experimental information is especially abundant for the praseodymium oxide–oxygen system, it is chosen here as the basis for developing a general structural model for defect fluorite-type phases. The PrO_2 parent is comprised of Pr^{4+} cations arranged in a f.c.c. array which interpenetrates with a simple cubic lattice of O^{2-} anions. In order to relate structures of the non-stoicheiometric PrO_x phases to that of PrO_2, it is neces-

[13] R. L. Martin, *Nature*, 1950, **165**, 202.
[14] D. J. M. Bevan, and J. Kordis, *J. Inorg. Nuclear Chem.*, 1964, **26**, 1509.
[15] D. J. M. Bevan, W. W. Barker, R. L. Martin, and T. C. Parks, ' Rare-earth Research,' ed. L. Eyring, Gordon and Breach, New York, 1965, vol. 3, p. 441.
[16] M. S. Jenkins, R. P. Turcotte, and L. Eyring, ' The Chemistry of Extended Defects in Non-metallic Solids,' eds. L. Eyring and M. O'Keeffe, North-Holland, Amsterdam, 1970, p. 36.
[17] C. A. Welsbach, *Monatsh.*, 1885, **6**, 477.
[18] B. G. Hyde and L. Eyring, ' Rare-earth Research,' ed. L. Eyring, Gordon and Breach, New York, 1965, vol. 3, p. 623.
[19] R. E. Ferguson, E. D. Guth, and L. Eyring, *J. Amer. Chem. Soc.*, 1954, **76**, 3890.
[20] H. S. Schuldt, Thesis, State University of Iowa, 1957.
[21] D. H. Everett and P. Nordon, *Proc. Roy. Soc.*, 1960, **A259**, 341.

sary to devise an alternative but convenient diagrammatic representation of anion vacancies in the $C1$ structure. Rather than the customary procedure

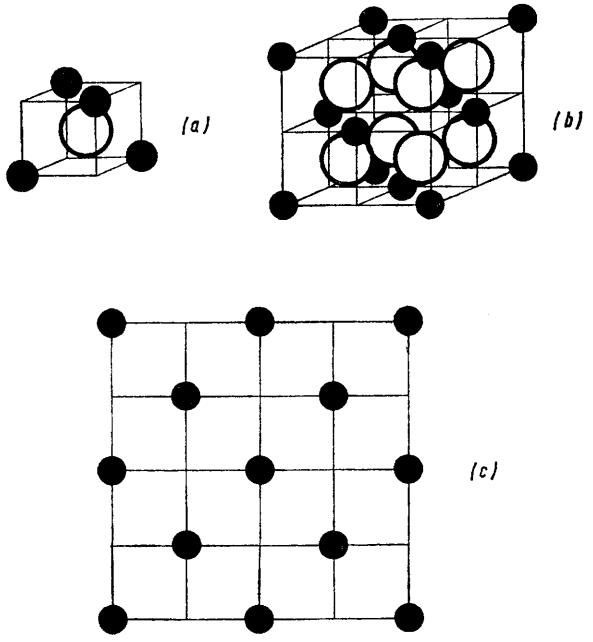

FIGURE 2 (*a*) Octant of composition Pr_4O; (*b*) $C1$ unit cell (eight octants) of composition Pr_4O_8; (*c*) Matrix representation for 16 octants (composition Pr_8O_{16})

of viewing the metal-centred polyhedra,[7,9] I focus attention on the orthogonal patterns of oxygen centred polyhedra.[10] The unit cell of PrO_2 [Figure 2(*b*)] is then an assembly of eight octants each with an O^{2-} ion at its body centre and being co-ordinated tetrahedrally by Pr^{4+} ions located at alternate corners of the octant [Figure 2(*a*)]. Each octant of composition Pr_4O and dimension $\frac{1}{2}a_{cub.}$ shares all its faces with similar octants to give an infinite array in three dimensions. If attention is directed to a single two-dimensional layer, the $C1$ structure can be represented in projection by the square matrix of octants of the fluorite cube [Figure 2(*c*)]. The face-centred array of Pr^{4+} ions is arranged at appropriate intersections of the matrix; O^{2-} ions are situated at the centre of each square.

Reduced praseodymium oxides result by removal of O^{2-} ions from octant centres thereby generating anion vacancies in the oxygen lattice according to equation (1),

$$4Pr^{4+} + O^{2-}/\square an \longrightarrow 4Pr^{4+} + 2e^-/\square an + \tfrac{1}{2}O_2 \rightleftharpoons 2Pr^{4+} + 2Pr^{3+} + \square an + \tfrac{1}{2}O_2 \quad (1)$$

where the symbol $\square$ is employed to designate an oxygen denuded site. Electrostatic balance in the lattice is preserved either by trapping electrons at the vacancy or by a reduction in oxidation state from IV to III for two of the four associated praseodymium cations.

Ions in the vicinity of the vacant anion site will be polarized as if the vacancy carried a virtual positive charge. For example, single-crystal X-ray studies of $Zr_3Yb_4O_{12}$ reveal consistent lengthening of M–M and shortening of O–O distances around the vacant anion site.[22] It is proposed here that the oxygen lattice is so highly polarized in the immediate neighbourhood of the $Pr_4\square$ defect, that the vacancy becomes strongly octahedrally co-ordinated by its six nearest O^{2-} neighbours [Figure 3(*a*)]. In other words, it is proposed that the point defect $\square$ has no independent existence in the fluorite lattice but, in its co-ordinated state $\square O_6$, it is a structural entity of very considerable thermodynamic stability. Indeed, it does appear to exert the dominant influence in determining the structures, compositions, phase relations, and reactions of non-stoicheiometric compounds based on anion-deficient fluorite structures of the lanthanoids.

The co-ordination defect. Before proceeding to an examination of the structural role played by the co-ordination, $\square O_6$, defect (c.d.), it is necessary to establish its total chemical composition as an independent entity. Since it is known that the cation lattice remains essentially intact, the true defect is constituted effectively of the seven octants which circumscribe the anion vacancy and each of its six nearest O^{2-} neighbours [Figure 3(*b*)]. The composition of this entity is $Pr_{\frac{7}{2}}\square O_6$ which corresponds to the formula, based on a fractional ratio of oxygen to metal, of $PrO_{1.714}$. It is significant that the ordered non-stoicheiometric phase of greatest thermal stability has identical composition

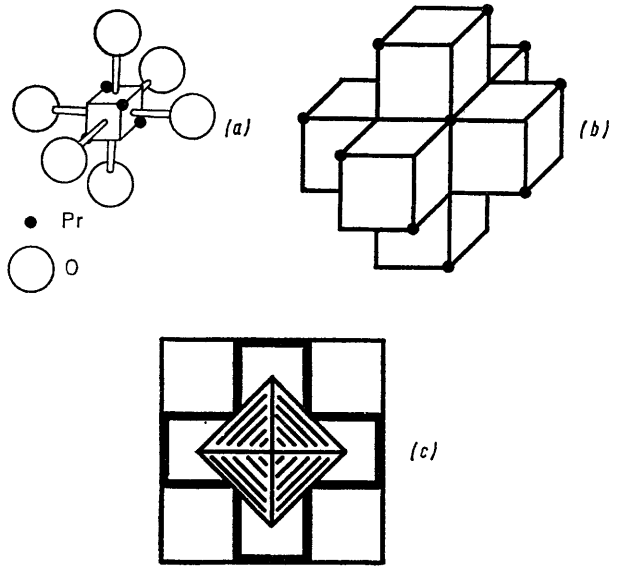

FIGURE 3 (*a*) Idealized stereochemical environment of vacant anion site; (*b*) idealized topology of c.d. with the composition $Pr_{\frac{7}{2}}\square O_6$; (*c*) octahedrally co-ordinated anion vacancy $\square O_6$ in projection on PrO_2 matrix

(*cf.* Table 1). The proposal that this composite structural unit retains its integrity in both low- and high-temperature phases in the range $PrO_{1.7}$—$PrO_{2.0}$, and is also the fundamental building block on which all the structures are based, follows naturally.

[22] M. R. Thornber and D. J. M. Bevan, *J. Solid-state Chem.*, 1970, **1**, 536.

The presence of a c.d. in a layer of the idealized fluorite lattice can be illustrated by extension of the matrix representation of Figure 2(*c*). The vacant anion site is

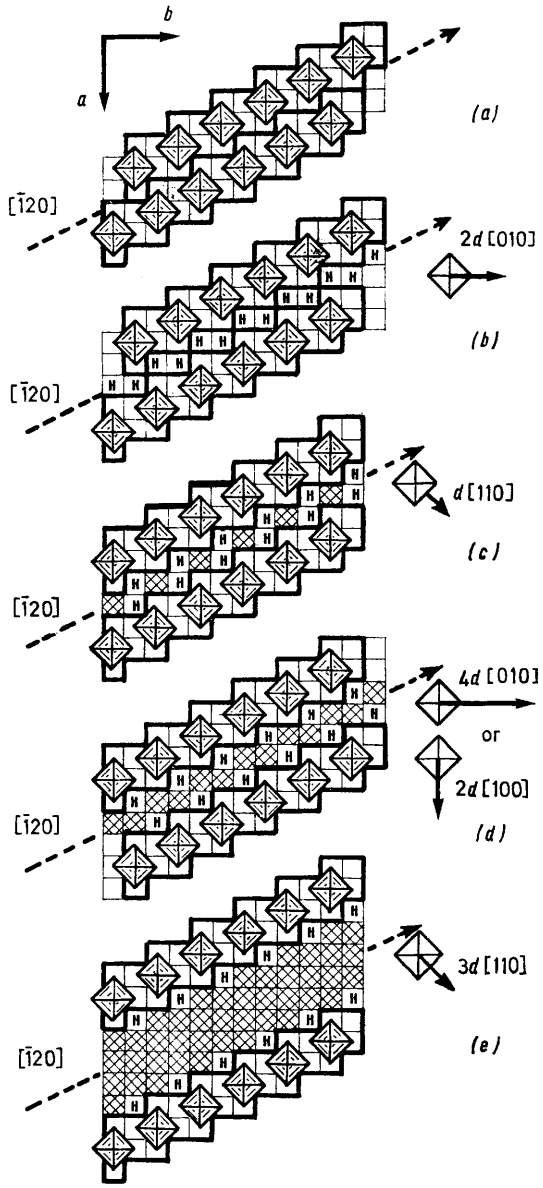

FIGURE 4 (*a*) Close packing of [1̄20] rows of c.d.s. in (001) plane; (*b*) mating holes H created in (001) plane by employing a shear vector $2d$[010]; (*c*), (*d*), and (*e*) creation of vacant sites (cross-hatched cubes) to accommodate additional Pr_4O octants required for compositions Pr_nO_{2n-2}

located at the centre of the O_6 octahedron shown in projection in Figure 3(*c*). In this convention it must be remembered that, while four of the six circumscribing octants are contained equatorially within a single layer, the remaining two axial octants must project into the two contiguous layers situated above and below the anion vacancy. It follows that the topology of the c.d. must predetermine and restrict the manner in which successive defect fluorite layers may be arranged so that all the octants complete a close-packed array and preserve the perfect cation lattice.

I proceed now to consider whether $Pr_{\frac{3}{4}}\square O_6$ might be the progenitor of the well defined homologous series of ordered praseodymium oxides Pr_nO_{2n-2} ($n = 7$ and 9—∞).

Structure and composition of ι-$PrO_{1.714}$. This is an ordered phase of narrow composition limits and is stable over a wide range of temperature and oxygen pressure for the binary Ce, Pr, and Tb oxygen systems. The ideal composition corresponds to M_7O_{12}; *i.e.* $n = 7$ in the M_nO_{2n-2} homologous series. *X*-Ray powder diagrams have been indexed on the basis of rhombohedral distortion of the *C*1 structure with dimensions of a pseudo-unit cell, $a = 5{\cdot}5096$ Å and $\alpha = 89{\cdot}63°$. This phase exhibits relatively strong superstructure reflexions which can be indexed[7] in terms of a true unit cell with $a = 6{\cdot}741$ Å and $\alpha = 99{\cdot}28°$. From these data the model in which two oxygen atoms are removed from Pr_7O_{14} along one of the four $\langle 111\rangle_{cub.}$ directions of the *C*1 structure has tentatively been proposed.[7] Although this model yields the correct stoicheiometry, and would promote rhombohedral distortion, the proposal provides little insight into the exact nature of the superstructure or the driving force which orders the anion vacancies. However, these features emerge from a consideration of the manner in which $Pr_{\frac{3}{4}}\square O_6$ c.d.s can be arranged in three dimensions.

Closest packing of c.d.s which can be achieved within a single layer of thickness d is illustrated in Figure 4(*a*). The resulting linear array lies along the [1̄20] direction. Rows of c.d.s can be arranged so that close packing is achieved by aligning the rows parallel to the [1̄20] direction. However, the stacking of additional layers

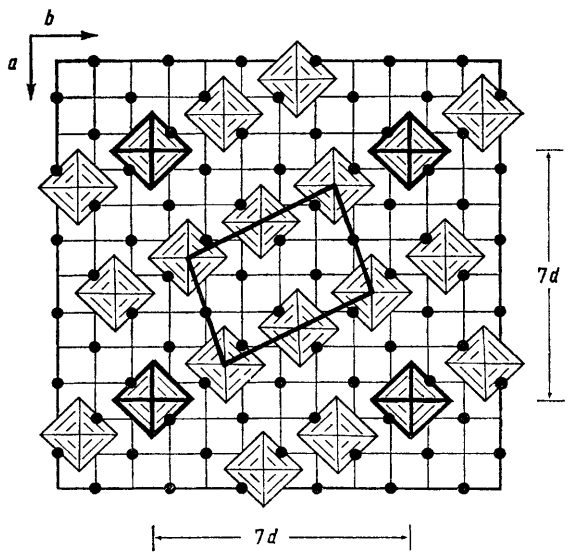

FIGURE 5 Idealized square-planar ($7d \times 7d$) cell for ι-$PrO_{1.714}$. A crystallographic translational unit of composition Pr_7O_{12} is outlined in black

up the *c* axis is precluded by steric hindrance due to axial octants situated above and below each vacancy. This problem can be overcome if the lower [1̄20] row

is sheared sequentially along the [010] direction by distance $2d$. This creates the necessary number (*i.e.* two) of vacant sites within each layer to enable axial octants of every c.d. to be mutually accommodated in contiguous layers. These newly created 'mating' holes in the *C*1 structure are labelled H in Figure 4 to avoid confusion with normal anion vacancies in the oxygen lattice. The ordering of anion vacancies which results from close packing of c.d.s within any (001) plane is illustrated in Figure 5. An idealized square-planar cell is delineated by the four marked c.d.s: each dimension is $7d$ (or *ca.* 19 Å) and encloses an overall chemical composition $Pr_{49/2}\square_7O_{42}$, *i.e.* $PrO_{1\cdot714}$.

Since tetrahedral groups of metal atoms may lie in either a right- or left-handed orientation [*cf.* Figure 2(*a*)], metal-atom positions in, say, the bottom layer of the square-matrix diagram have been included in Figure 5 to show that the translational repeat distance of the metal sub-lattice is $2d$. As a result the square-planar cell is only a unit of composition, but not a crystallographic repeat unit: adjacent cell corners have opposite-handed c.d.s, as they must for any translational step of $(2n + 1)d$, where $d = \frac{1}{2}a_{cub.}$ A true crystallographic-translation unit of the correct phase is outlined in black (Figure 5) and possesses the chemical composition $Pr_7\square_2O_{12}$ of the ι-phase.

In this representation, seven additional (001) layers must be superimposed along the *c* axis to complete the idealized cubic $(7d \times 7d \times 7d)$ unit of chemical composition $Pr_{343/2}\square_{49}O_{294}$, illustrated in isometric projection in Figure 6(*a*). Because superimposition of layers [*cf.* Figure 4(*b*)] is subject to the requirement that the Pr–Pr tetrahedron edges must mate up between themselves, a displacement of $d[\bar{2}11]$ from one layer, as drawn, to the next is involved as each of the seven layers is added successively. In this three-dimensional assembly of octants, the true crystallographic repeat unit is expected to be rhombohedral, there being a 3-fold axis along $[\bar{1}\bar{1}1]$, with the c.d.s which define the corners of any one face lying in three different octant-stacking layers.

The nature of the superstructure generated by this topologically determined ordering of c.d.s now becomes apparent. Since each point defect is operated on by the translation vector $d[\bar{2}11]$ as seven layers are added consecutively to the *ab* plane, it is a necessary consequence that vacancies in the oxygen lattice are wholly contained in families of {213} planes with an interplanar spacing of $7d/\sqrt{14}$ [Figure 6(*b*)]. Fine detail of the superstructure of ordered anion vacancies within a single (213) plane is illustrated in Figure 6(*c*). It is uniquely determined by the topology of the $Pr_{\frac{7}{8}}\square O_6$ c.d. and requirements imposed by close packing to generate a completed cation sub-lattice. Short- or long-range forces of other kinds do not appear to play a dominant role in determining the structure of this ordered non-stoicheiometric phase.

In this analysis, earlier descriptions, based on ordering of anion vacancies into 'strings' or 'pairs' parallel to one of the $\langle 111\rangle_{cub.}$ directions of the ideal fluorite lattice, are consequential on the operation of the translation vector $d[\bar{2}11]$. However, it is significant that anion vacancies are necessarily confined to the oblique {213} rather than {111} planes as might have been speculated on the basis of Caro's [10,11] analysis. Furthermore, the observed oxygen : metal ratio of 1·714 : 1 is a direct result of very strong short-range forces rather than arising from arbitrary omission of two oxygen atoms along a [111] trigonal axis of Pr_7O_{14}.

It appears that the polarizing power of the $Pr_4\square$ core is largely saturated by the immediate environment of six O^{2-} ions and that residual short-range interactions, with the 12 next-nearest O^{2-} neighbours at $d\sqrt{2}$ and the eight next-next-nearest O^{2-} neighbours at $d\sqrt{3}$, exert no significant influence on the ordering of anion vacancies.

The packing of $Pr_{\frac{7}{8}}\square O_6$ c.d.s uniquely determine this structure so that ordered phases of similar composition are to be anticipated in other binary and related ternary systems. Indeed, several M_7O_{12} binary phases have been reported for M = Ce [23] and Tb,[6,24] as well

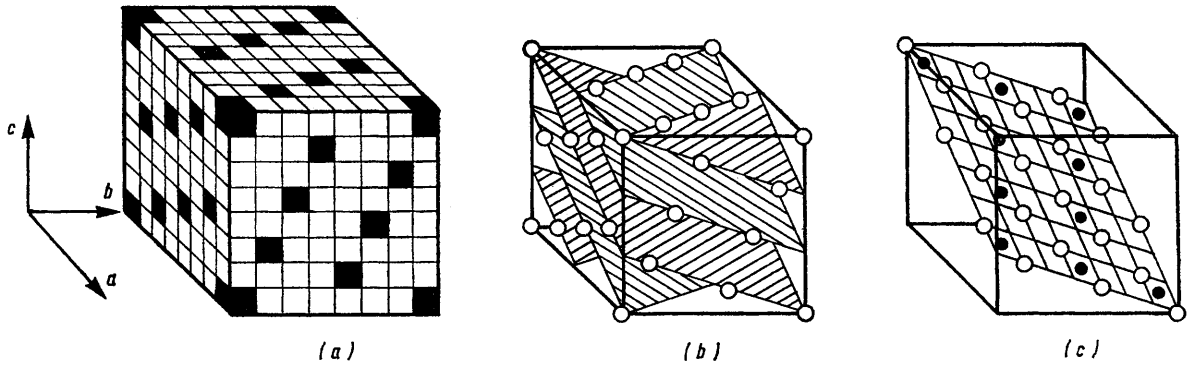

FIGURE 6 (*a*) Isometric projection of idealized cubic cell $(7d \times 7d \times 7d)$ for ι-$PrO_{1\cdot714}$ (vacant octants are marked in black); (*b*) orientation of five {213} oxygen defect planes (interplanar spacing = $7d/\sqrt{14}$); (*c*) location of vacant oxygen sites and metal atoms (●) on a single (213) plane

[23] D. J. M. Bevan, *J. Inorg. Nuclear Chem.*, 1955, **1**, 49.
[24] E. D. Guth and L. Eyring, *J. Amer. Chem. Soc.*, 1954, **76**, 5242.

as a variety of ternary rhombohedral phases of the general type [25-27] $M = (W_{\frac{1}{7}}Y_{\frac{9}{7}})$, $(U_{\frac{1}{7}}Lu_{\frac{9}{7}})$, $(U_{\frac{2}{7}}Y_{\frac{5}{7}})$, and $(Zr_{\frac{3}{7}}Ln_{\frac{4}{7}})$ (Ln = Sc, Tm, or Yb [9,22,28,29]). Interestingly, $Zr_3Sc_4O_{12}$ appears to be isomorphous with the phase [30] $Zr_7O_8N_4$ which conceivably could involve either *cis*- or *trans*-$\square N_2O_4$ co-ordination of anion vacancies. In the case of $Zr_3Sc_4O_{12}$ *X*-ray powder-diffraction data have been interpreted in terms of rhombohedral distortion of the fluorite lattice with one cubic [111] direction becoming the unique inversion triad axis of the $R\bar{3}$ space group.[9] Subsequently, the same authors [22] obtained single-crystal *X*-ray data for $Zr_3Yb_4O_{12}$ and established that partial ordering of Zr^{4+} and Yb^{3+} ions in the cation lattice occurs in the low-temperature form and confirmed the expectation that neighbouring oxygen atoms are drawn in towards the vacant anion sites. The remarkable resistance to further reduction of this ι-phase provides convincing evidence of the strong intrinsic requirement for octahedral anion co-ordination about each $Pr_4\square$ defect to be preserved. The ι-$PrO_{1.714}$ phase ultimately decomposes peritectoidally to the non-stoicheiometric σ-phase at 1 054 °C at an oxygen pressure of 59_2 Torr.

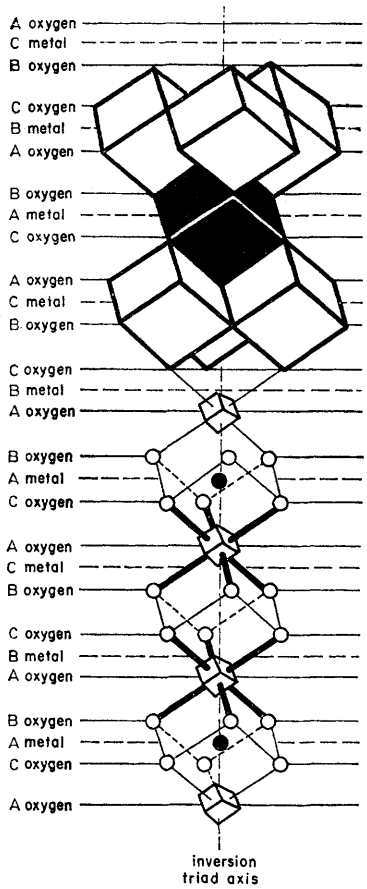

FIGURE 7 M_7O_{36} defect cluster and the octahedrally co-ordinated anion vacancy $\square O_6$ delineated in the same [111] infinite 'string'

Interrelations between the infinite linear 'string,' the M_7O_{36} structural sub-unit, and the present c.d. models emerge from a comparison of Figure 1(*b*) with 7. In the latter the M_7O_{36} defect cluster [7,9] and the octahedrally co-ordinated anion vacancy $\square O_6$ of Figure 3(*a*) are delineated in the same [111] linear 'string.' The M_7O_{36} defect cluster is comprised of six metal-centred MO_7 polyhedra (white cubes) and a central MO_6 polyhedron (black cube) with a pair of vacant oxygen sites disposed across its [111] body diagonal. In contrast, the $M_{\frac{7}{2}}\square O_6$ c.d. is comprised of six intact Pr_4O anion-centred octants surrounding a central defect octant $Pr_4\square$ in an octahedral configuration. If two c.d.s are mated so that the two vacant sites lie on a ⟨111⟩ axis, the resulting pair have the chemical composition $Pr_7\square_2O_{12}$ and essentially represent the anion-centred image of the M_7O_{36} structural sub-unit. However, the present concept of octahedral co-ordination of the point defect appears to offer a deeper insight into anion-deficient structures. Not only is an origin for the short-range forces suggested, but also the nature of the superstructure can be identified in terms of a convenient diagrammatic representation employing a square matrix of octants of the fluorite cube. This leads directly to the proposition that infinite linear 'strings' or 'pairs' of vacancies are gathered into sheets on {213}. Importantly, it will be seen in the following sections that the chemical composition of any MO_x phase is more readily ascertained in the anion-centred representation.

Structure and composition of other Pr_nO_{2n-2} *phases.* More oxidized phases are also characterized by a narrow homogeneity range (*cf.* Table 1) and comprise the higher homologues with $n = 9—\infty$; the member with $n = 8$ appears to be missing. Unfortunately, the series classification in itself provides only limited

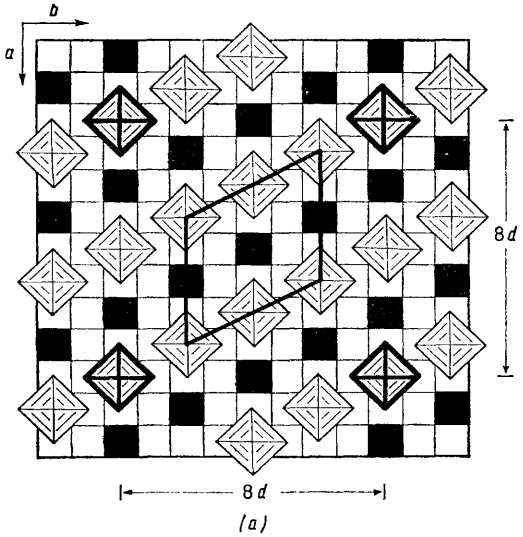

FIGURE 8

[25] H. J. Borchardt, *Inorg. Chem.*, 1961, **2**, 170.
[26] G. A. Chase, *Acta Cryst.*, 1962, **15**, 91.
[27] S. F. Bartram, *Inorg. Chem.*, 1966, **5**, 749.
[28] M. Perex y Jorba, *Ann. Chim.* (*France*), 1963, **8**, 117.
[29] J. LeFèvre, *Ann. Chim.* (*France*), 1963, **8**, 135.
[30] J. C. Gilles, *Corrosion et Anticorrosion*, 1964, **12**, 15.

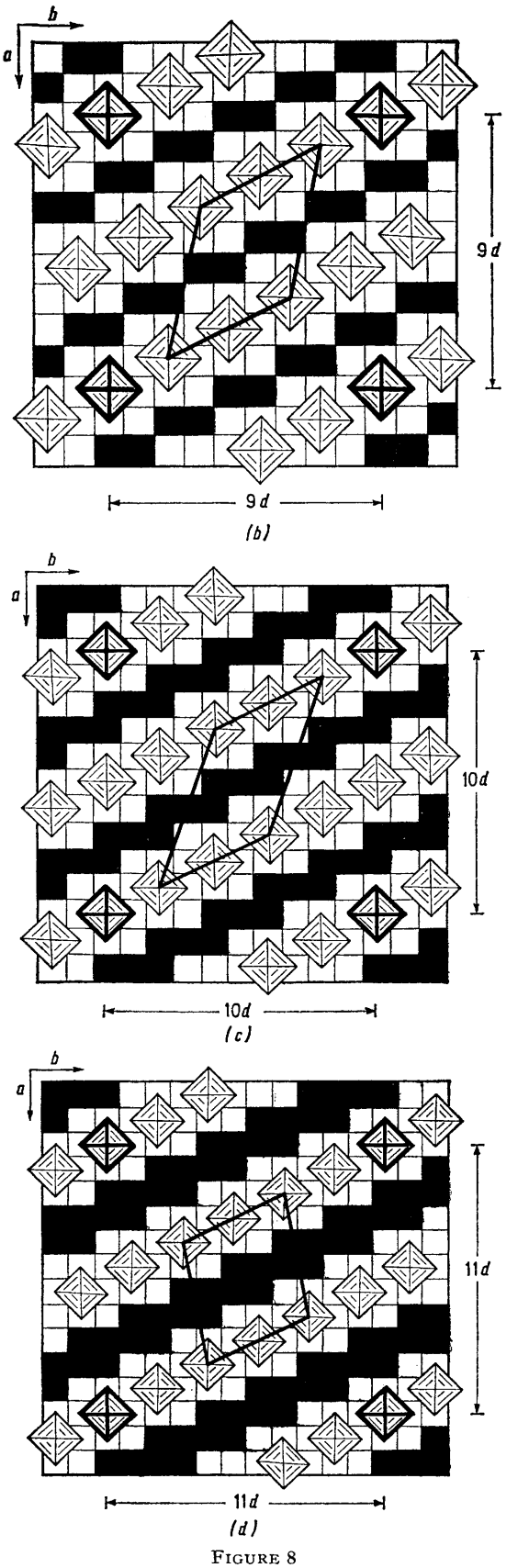

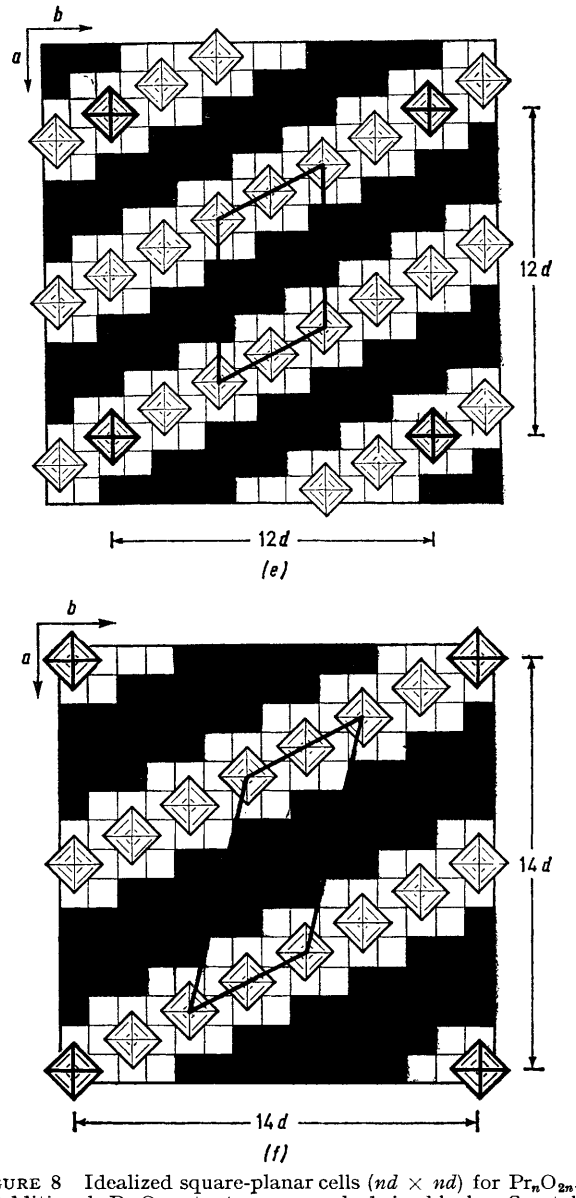

FIGURE 8 Idealized square-planar cells ($nd \times nd$) for Pr_nO_{2n-2}. Additional $Pr_{\frac{1}{4}}O$ octants are marked in black. Crystallographic translation units of composition Pr_nO_{2n-2} are outlined in black: (*a*) $PrO_{1\cdot75}$ ($8d \times 8d$); (*b*) ζ-$PrO_{1\cdot78}$ ($9d \times 9d$); (c) ε-$PrO_{1\cdot800}$ ($10d \times 10d$); (*d*) δ-$PrO_{1\cdot818}$ ($11d \times 11d$); (*e*) β-$PrO_{1\cdot833}$ ($12d \times 12d$); (*f*) $PrO_{1\cdot857}$ ($14d \times 14d$)

insight into the genesis of these phases: *i.e.* their composition, structure, and underlying mechanism of formation. However, simple extension of the topological analysis applied to ι-Pr_7O_{12} yields structures with compositions which conform to Pr_nO_{2n-2} and offers more-detailed insight into the nature of the ordering of anion vacancies on which the superstructures are based.

The primitive composition of each homologue in Table 1 may be obtained by adding y octants of $Pr_{\frac{1}{4}}O$ to the c.d. $Pr_{\frac{7}{2}}\square O_6$ ($y = 1—\infty$). The composition of each phase is then $Pr_{\frac{7}{2}+\frac{1}{2}y}\square O_{6+y}$ or $Pr_nO_{2n-2}\square_2$ ($n = y + 7$). Although it has been claimed [5] that the

sesquioxide Pr_2O_3 is a member of this series (*i.e.* with either $n = 4$ or $y = -3$), its structure is based on ordered omission of anions quite different in concept to the superlattices proposed below for the higher homologues.

The concomitant topological problem is to deduce the manner in which additional octants of $Pr_{\frac{1}{2}}O$ may be incorporated into the type-ι structure whilst preserving the cation lattice intact. An obvious solution is to increase the spacing between the rows of c.d.s which lie along [$\bar{1}$20] directions within any (001) layer, subject to the additional constraint imposed by the need to phase the cation sub-lattice correctly. For example, operation of the shear vectors d[110], $4d$[010], and $3d$[110] on the lower strand of c.d.s of Figure 4(*a*) creates 3, 4, or 9 additional cavities which, when filled by $Pr_{\frac{1}{2}}O$ octants, yield compositions Pr_8O_{14} ($n = 8$), each $Pr_{\frac{7}{2}}\square O_6$ c.d. ensures that these structures are highly ordered since they retain all the packing characteristics of their ι-Pr_7O_{12} progenitor, except that each ι-Pr_7O_{12} layer becomes progressively removed from its neighbouring layers by a sheet-like intergrowth of PrO_2 of increasing width. At the composition $Pr_{14}O_{26}$, each layer of ι-Pr_7O_{12} is interleaved with a layer of Pr_7O_{14} of exactly the same topology and dimensions. Thus at more oxidized compositions, the true progenitor is better regarded as the fluorite matrix of PrO_2 in which sheets of ι-Pr_7O_{12} become progressively diluted. The triclinic symmetry of these homologues, which is apparent in *X*-ray powder photographs,[7] is to be anticipated from the low symmetry associated with anisotropic ordering of c.d.s in the cubic PrO_2 matrix. However, the lowering of symmetry should attenuate as the value of x in PrO_x approaches 2.

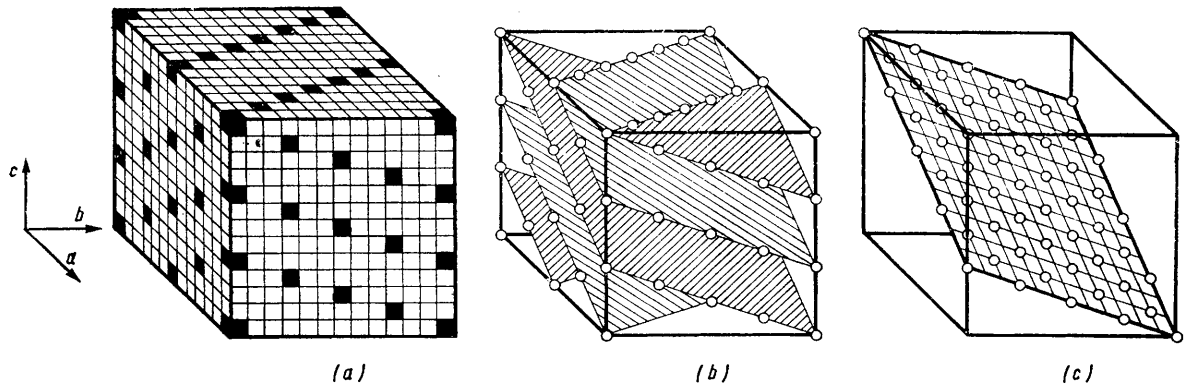

FIGURE 9 (*a*) Isometric projection of idealized cubic cell ($12d \times 12d \times 12d$) for β-$PrO_{1.833}$ (vacant octants are marked in black); (*b*) orientation of five (213) oxygen defect planes (interplanar spacing = $12d/\sqrt{14}$); (*c*) location of vacant oxygen sites on a (213) plane

Pr_9O_{16} ($n = 9$), and $Pr_{14}O_{26}$ ($n = 14$) [*cf.* Figures 4(*c*), 4(*d*), and 4(*e*)]. Layers of the square-planar cells [(001)] for $PrO_{1.750}$, ζ$PrO_{1.778}$, ε-$PrO_{1.800}$, δ-$PrO_{1.818}$, β-$PrO_{1.833}$, and $PrO_{1.857}$ derived from this structural principle are illustrated in Figure 8. The square-cell dimension increases linearly as the ordered phase becomes progressively more oxidized in accord with

TABLE 2

Data for idealized cubic cells of Pr_nO_{2n-2}

x = O : Pr	Composition of one square-planar cell	Oxygen vacancies : oxygen sites	Volume of cubic cell (d^3)	$Pr_{\frac{7}{2}}\square O_6$: $Pr_{\frac{1}{2}}O$
1·714	$Pr_{49/2}\square_7O_{42}$	$\frac{1}{7}$	7^3	7 : 0
1·750	$Pr_{32}\square_8O_{56}$	$\frac{1}{8}$	8^3	8 : 8
1·778	$Pr_{81/2}\square_9O_{72}$	$\frac{1}{9}$	9^3	9 : 18
1·800	$Pr_{50}\square_{10}O_{90}$	$\frac{1}{10}$	10^3	10 : 30
1·818	$Pr_{121/2}\square_{11}O_{110}$	$\frac{1}{11}$	11^3	11 : 44
1·833	$Pr_{72}\square_{12}O_{132}$	$\frac{1}{12}$	12^3	12 : 60
1·857	$Pr_{98}\square_{14}O_{182}$	$\frac{1}{14}$	14^3	14 : 98

the stoicheiometry Pr_nO_{2n-2}. Chemical compositions of the square-planar cells for these phases are summarized in Table 2.

The special topological requirements for stacking successive layers to accommodate the two axial cubes of

Finer details of the superstructures which emerge for these ordered phases in this composition region can again be revealed better by isometric representation of one of the more-oxidized cubic unit cells. The structure derived for β-$Pr_{12}O_{22}$ is sketched in Figure 9(*a*), oxygen-denuded octants (the sites of anion vacancies) being marked in black. The (001) face displays the basic two-dimensional ordering of c.d.s illustrated in Figure 8(*e*). However, the pattern of defects on the (100) and (010) faces differs due to coherent intergrowth of PrO_2 between (213) planes of anion vacancies. Five of these (213) planes spaced at $12d/\sqrt{14}$ are sketched in Figure 9(*b*). The exact ordering of anion vacancies in one of the (213) planes of β-$Pr_{12}O_{22}$ shown in Figure 9(*c*) is identical to that for ι-Pr_7O_{12} [Figure 6(*c*)], and is common to all the homologues. Superstructures of the *C*1 lattice for the ordered homologues differ only in thickness of the PrO_2 intergrowth as defined by the interplanar spacing $nd/\sqrt{14}$ of anion vacancies contained in (213) planes. Clearly the homologous composition determined experimentally, $Pr_nO_{2n-2}\square_2$, simply reflects the separation of consecutive (213) planes of anion vacancies by (n − 1) parallel planes filled with oxide ions.

Higher-temperature phases. PrO_2 Is known [31] to be completely dissociated at 378 °C at an oxygen pressure of 65 p.s.i. If the ordered low-temperature phases Pr_nO_{2n-2} are based on intergrowths of PrO_2 and ι-Pr_7O_{12}, then it might be anticipated that the homologues would decompose at lower temperatures as the proportion of PrO_2 increases. Approximate peritectoid oxygen pressures and temperatures [5] are summarized in Table 3.

TABLE 3

Peritectoid pressures and temperatures [a]

Equilibrium	Oxygen pressure Torr	T/K	Mole fraction Pr_7O_{12} : PrO_2
(A) $Pr_{12}O_{22} \rightleftharpoons \beta' + \alpha$	$5{\cdot}5 \times 10^4$ [b]	749	1 : 5
(B) $2Pr_{11}O_{20} \rightleftharpoons \beta' + Pr_{10}O_{18}$	13_7	750	1 : 4
(C) $3Pr_{10}O_{18} \rightleftharpoons \beta' + 2Pr_9O_{16}$	38	792	1 : 3
(D1) $4Pr_9O_{16} \rightleftharpoons \beta' + 3Pr_8O_{14}$	*c*	*c*	1 : 2
(D2) $5Pr_9O_{16} \rightleftharpoons 2\beta' + 3Pr_7O_{12}$	26	881	1 : 2
(E) $5Pr_8O_{14} \rightleftharpoons \beta' + 4Pr_7O_{12}$	*c*	*c*	1 : 1
(F) $6Pr_7O_{12} \rightleftharpoons \beta' + 5\sigma$	59_2	1327	1 : 0

α, Wide-range, disordered, non-stoicheiometric phase PrO_x with $1{\cdot}72 \lesssim x \lesssim 2{\cdot}00$; β′, disordered $Pr_{12}O_{22}$; σ, wide-range, disordered, non-stoicheiometric phase PrO_x with $1{\cdot}6 \lesssim x \lesssim 1{\cdot}7$.

[a] Ref. 5. [b] 73 atm. [c] Not observed.

It is significant that when the published peritectoid temperatures are plotted as a function of the mol ratio $[Pr_7O_{12}] : [PrO_2]$, a linear relation is obtained (*cf.* Figure 10) consistent with the proposal of coherent intergrowth between the two progenitors.

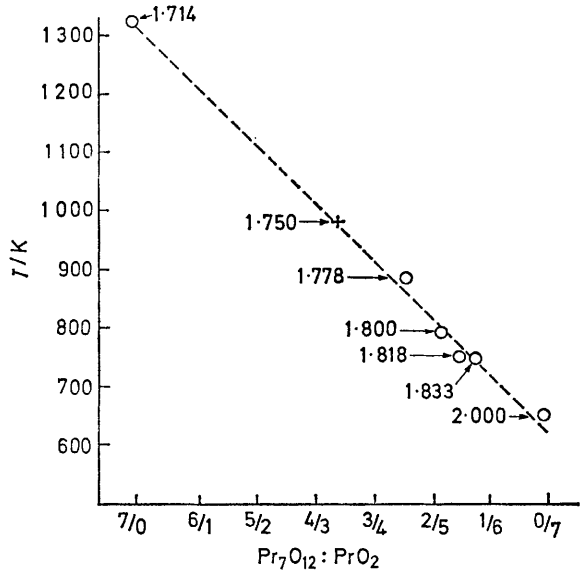

FIGURE 10 Peritectoid temperatures for PrO_x as a function of the mol ratio $Pr_7O_{12} : PrO_2$. Datum for $PrO_{1{\cdot}750}$ is interpolated

An ordered Pr_8O_{14} phase has been elusive in isobaric and tensimetric studies, although compositions as high as $PrO_{1{\cdot}74}$ have been observed [5] in oxidation isobars at oxygen partial pressures of *ca.* 1 atm at 900 °C. Interpolation of the data in Figure 10 suggests that Pr_8O_{14} would be expected to decompose peritectoidally at *ca.* 950 K if it exists. It appears, however, that below 881 K Pr_8O_{14} is metastable with respect to ζ-Pr_9O_{16} and ι-Pr_7O_{12} so that the anticipated reactions (D1) and (E) of Table 3 are simply replaced by overall equilibrium (D2). No structural reason can be advanced at this stage for the apparent instability of the Pr_8O_{14} phase; in terms of the present model it appears to differ from ι-Pr_7O_{12} and ζ-Pr_9O_{16} only in that successive (213) vacancy planes are separated by seven rather than six or eight oxygen-intact planes, respectively. Above 881 K, only the ι-Pr_7O_{12} and α-phases are found in this composition region.

Traditionally, the grossly non-stoicheiometric α-phase which overlays the Pr_nO_{2n-2} ordered homologues has been regarded as a single phase with anion vacancies randomly distributed in statistical manner. A recent combination of thermogravimetric isobaric analysis with high-temperature *X*-ray diffraction studies suggests [16] that the α-phase in the region $\sim 1{\cdot}785 \lesssim x \lesssim 1{\cdot}830$ can be resolved into four sub-regions designated as α_1, α_2, α_3, and α_4. It would appear that long-range order is not eliminated entirely at the higher temperatures and that the α-phase should not be regarded as fully disordered but rather as being somewhat less ordered than the homologues.

Ariya and Popov consider a non-stoicheiometric phase as consisting solely of regions or microdomains possessing characteristics of the lower and higher homologues which define the composition range.[32] Jenkins *et al.*[16] apply this concept of 'microheterogeneity' to interpret the texture of α-PrO_x as follows: α_1, microdomains of ε* coherently intergrown with ι*; α_2, δ* with ι*; α_3, β* with ι*; and α_4, fluorite* with ι*. The asterisk is employed to designate that α_1 is not simply a solution of ε + ι phases, but rather some structural unit which is characteristic of ε in the bulk phase and which persists into α_1. They suggest the domain texture would be very fine, perhaps <100 Å.

These observations find a natural explanation in terms of the present topological analysis of c.d.s. Reference to Figure 4 shows that incorporation of additional

TABLE 4

Shear vectors for generating [from Figure 4(*a*)] basic (001) layers of Pr_nO_{2n-2} (Figure 8) with correct phasing of the cation sub-lattice

Phase	Shear vector
ι-Pr_7O_{12}	$2d$[010]
Pr_8O_{14}	d[110]
ζ-Pr_9O_{16}	$4d$[010] or $2d$[100]
ε-$Pr_{10}O_{18}$	(d[110] + $2d$[010])
δ-$Pr_{11}O_{20}$	$6d$[010] or $2d$[110]
β-$Pr_{12}O_{22}$	(d[110] + $2d$[100])
$Pr_{13}O_{24}$	$8d$[010] or $4d$[100]
$Pr_{14}O_{26}$	$3d$[110]

Pr_4^1O octants in cavities H, created by employing translational vectors (*cf.* Table 4) which preserve the correct phase relations for the cation sub-lattice,

[31] H. A. Pagel and P. H. Brinton, *J. Amer. Chem. Soc.*, 1929, **51**, 42.

[32] S. M. Ariya and Yu G. Popov, *J. Gen. Chem.* (*U.S.S.R.*), 1962, **32**, 2077.

ensures that characteristic line defects for all the ordered phases can be matched along the [$\bar{1}$20] direction. Accordingly, it is possible for the composition of the non-stoicheiometric α-region to vary continuously by a process of coherent intergrowth of appropriate proportions of the two homologues which provide the boundaries of the α_1, α_2, α_3, and α_4 sub-regions. The composition of the α-phase can then be expressed as $Pr_{(n+\theta-1)}O_{2(n+\theta-2)}$, where θ is the mol fraction of the more oxidized homologue Pr_nO_{2n-2} which forms the

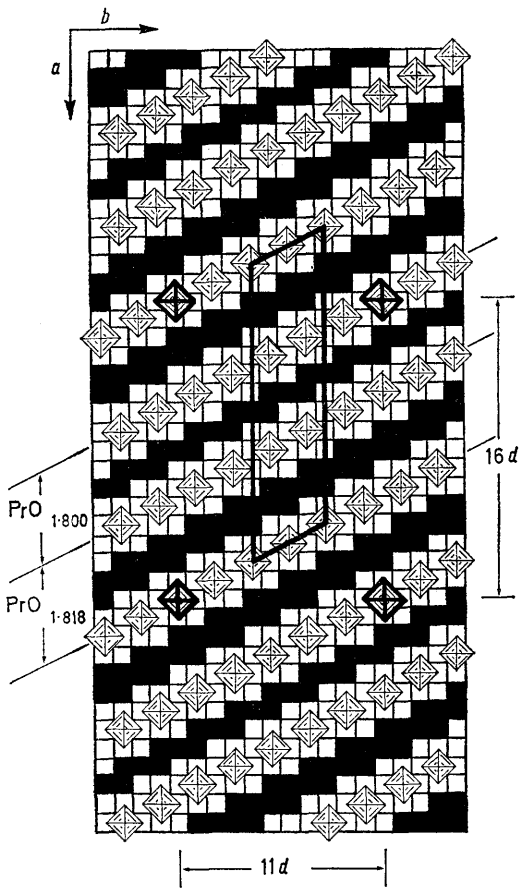

FIGURE 11 Ordered intergrowth of $PrO_{1\cdot818}$ and $PrO_{1\cdot800}$ in the ratio 2 : 1 to yield a non-stoicheiometric α-phase of composition $PrO_{1\cdot8125}$. A crystallographic translation unit of composition $Pr_{32}\square_6O_{58}$ is outlined in black

upper boundary of each α_i region. For example, an α_2-phase of composition $PrO_{1\cdot8125}$ would correspond to $\theta = \frac{2}{3}$ and $n = 11$. The structure of an (001) layer is illustrated in Figure 11. The composition of a rectangular cell of dimensions $11d \times 16d$ is $Pr_{96}\square_{18}O_{174}$ or $PrO_{1\cdot8125}$. Essentially it consists of an ordered intergrowth of $Pr_{11}\square_2O_{20}$ (δ-$PrO_{1\cdot818}$) and $Pr_{10}\square_2O_{18}$ (ε-$PrO_{1\cdot800}$) arranged so that successive sheets are stacked to preserve the ratio 2 : 1. The observed texture of the α_2-phase in this description would arise from microdomains of δ* [*i.e.* (213) sheets of the δ-phase] coherently intergrown with ε* [*i.e.* (213) sheets of the ε-phase].

This interpretation of coherent intergrowths enables a rational description of order–disorder transitions to be provided. Hyde *et al.*[5] have noted that neither order nor disorder in praseodymium oxides is ever complete. For example, their isobaric data establish that each of the homologues possesses a small homogeneity range, $\Delta x \pm 0{\cdot}003$, which is a natural consequence of coherence (*cf.* Table 1). Similarly, they point out that the homologous Pr_nO_{2n-2} ordered phases persist up to quite high temperatures, whereas the 'disordered' α-phase, in the same composition range, extends to much lower temperatures (a minimum of 456 °C). Thus three phases δ-$PrO_{1\cdot818}$, β-$PrO_{1\cdot833}$, and α are all observed in the narrow composition range $1{\cdot}81 < x < 1{\cdot}84$ at 460 °C. It is inconceivable that δ and β should possess a high degree of structural order and that α should be perfectly disordered. However, coherent intergrowth between the two homologues bounding any composition region leads to an α-phase of any composition but retaining considerable structural order. In effect, the regular spacing of (213) defect planes which characterizes the ordered phases becomes progressively randomized (interplanar disorder). At the same time, each defect plane can retain the high degree of structural order which is characteristic of the homologues (intraplanar order).

Intraplanar order which remains in the α-phase is consistent with the conclusion of Hoch and Yoon [33] that the critical temperature $T_c = E_{vv}/2R = 30\,000$ K deduced from a random anion-vacancy model for the α-phase of CeO_2 ($1{\cdot}8 < x < 2{\cdot}0$) is totally incompatible with the observed value 958 K. It is significant that coherence between two phases has been shown to depress drastically the critical temperature T_c of Au–Ni alloys.[34] The observation [20] that oxidation and reduction of PrO_x phases are not accompanied by changes in surface area and the occurrence of hysteresis in some of the phase transformations [5,12] are likewise consistent with the proposal of coherent intergrowth.

The present concept of planar ordering of anion vacancies in these materials differs from the process of crystallographic shear for accommodating non-stoicheiometry of some transition-metal oxides in that the (213) sheets of defects can be finite, and terminated without distortion by substituting $M_4\square$ positions by intact M_4O octants. The transition from order to disorder can then be visualized in terms of the progressive randomization:

Ordered spacing of infinite (213) sheets of $Pr_{\frac{2}{3}}\square O_6$ in a matrix $Pr_{\frac{2}{3}}O_7$ → Randomized spacing of infinite (213) sheets → Mixing of defect sheets with PrO_2 slab material to give finite discs of $Pr_{\frac{2}{3}}\square O_6$

Disordering of defects in (213) *planes.* The principal feature of the preceding analysis is the gathering and preservation of anionic vacancies on (213) planes.

[33] M. Hoch and H. S. Yoon, 'Rare-earth Research,' ed. L. Eyring, Gordon and Breach, New York, 1965, vol. 3, p. 665.
[34] J. W. Cahn, *Acta Metallurgica*, 1961, **9**, 795.

The most disordered phase would correspond to finite discs of $Pr_{\frac{7}{2}}O_6$ contained in irregularly spaced (213) planes. However, there are alternative and less-ordered ways of distributing oxygen vacancies throughout the *C*1 structure. This arises because the overall topologies of $Pr_{\frac{7}{2}}\square O_6$ and $Pr_{\frac{7}{2}}O_7$ are identical so that any composition PrO_x in the range $1{\cdot}714 < x < 2{\cdot}000$ may be achieved simply by varying the proportions of

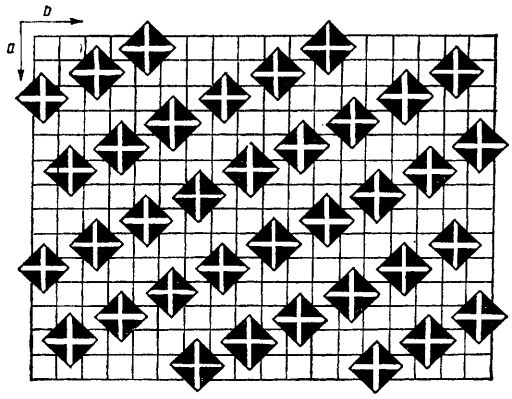

FIGURE 12 Idealized two-dimensional sheet of PrO_2 with topology identical to that of ι-$PrO_{1{\cdot}714}$ and ordered as illustrated in Figure 5 ($Pr_{\frac{7}{2}}O_7$ marked as black octahedra in projection)

each component; *i.e.* $\theta Pr_{\frac{7}{2}}\square O_6 + (1-\theta)Pr_{\frac{7}{2}}O_7 \equiv Pr_{\frac{7}{2}}\square_\theta O_{7-\theta}$, where $0 < \theta < 1$. In this representation, the homologues $n = 7$—∞ correspond to values of $\theta = 7/n$.

Anion vacancies on (213) planes can be visualized as being progressively randomized in either or both of two ways.

(*i*) If the $Pr_{\frac{7}{2}}\square O_6$ c.d.s are confined to (001) planes (Figure 5) and the $Pr_{\frac{7}{2}}O_7$ units to (001) planes (Figure 12), then any composition PrO_x can be achieved by stacking the two types of layer along the *c* axis in appropriate proportions and the required order. For example, if single layers of each type are stacked in an alternating sequence following the procedure outlined earlier for ι-Pr_7O_{12}, a composition $Pr_{14}O_{26}$ is obtained in which the [$\bar{1}$20] rows of vacancies remain intact. However, each alternate row on a (213) plane is necessarily annihilated so that all metal atoms on three-fold axes now lie in seven- rather than six-co-ordinated sites.

Although a praseodymium oxide phase of this composition has not been isolated, ternary compounds with this stoicheiometry have been reported. These include $Zr_{10}Sc_4O_{26}$,[9,29] $Zr_{14}O_{22}N_4$,[30] and possibly the 'rhombohedral 2' phase observed in the U + Y + O system.[27] The structure of $Zr_{10}Sc_4O_{26}$ has been determined from Hägg–Guinier focussing *X*-ray powder photography by assuming a model based on rhombohedral distortion of the *C*1 structure along one of the ⟨111⟩ cubic directions. In the case of $Zr_3Sc_4O_{12}$ all oxygen sites on the three-fold rotation axes were assumed to be vacant [*cf.* Figure 1(*b*)]. However, for $Zr_{10}Sc_4O_{26}$ the model which refines best has one half of these sites occupied and one half vacant [*cf.* Figure 1(*c*)]. Furthermore, filled and unfilled oxygen positions occur in a pairwise sequence making the cations located on the three-fold axis alternately six- and eight-co-ordinate.[9]

Essential features of this structure are reproduced by alternately stacking two layers of $Pr_{\frac{7}{2}}\square O_6$ followed by two layers of $Pr_{\frac{7}{2}}O_7$ employing the translation vector $d[\bar{2}11]$ as outlined earlier. The resulting density of point defects in any denuded (213) plane is now halved since each alternate pair of [$\bar{1}$20] strings of anion vacancies along [$\bar{1}\bar{1}$1] has been eliminated by intergrowth of $Pr_{\frac{7}{2}}O_7$ (Figure 13). We must infer that, at least for the ternary $Zr_{10}Sc_4O_{26}$ phase, a structure based on intact (213) vacancy planes separated by $14d/\sqrt{14}$ is less favoured thermodynamically than the real structure in which the number of vacancies per (213) plane is halved but the frequency of their occurrence is doubled; *i.e.* half-filled (213) planes now occur at a spacing of $7d/\sqrt{14}$ characteristic of the ι-Pr_7O_{12} phase. It cannot be ascertained at this stage whether this structure is a reflection of a preference for pairing of vacant anion sites as in the M_7O_{36} defect complex or whether cation ordering is the feature which determines the preferred order of stacking of $M_{\frac{7}{2}}\square O_6$ moieties. Thus Thornber and Bevan [22] determined the structure of the low-temperature form of $Zr_3Yb_4O_{12}$ from single-crystal *X*-ray studies and established that the smaller, more highly charged, Zr^{4+} ions have a distinct preference for MO_6 co-ordination sites.

In summary, the defect occupancy factor for any (213) plane is given by $\theta = 7/n$; *i.e.* vacant anion sites are confined to $7/n$ of the *n* original [$\bar{1}$20] rows on (213) planes separated by the distance $7d/\sqrt{14}$ characteristic

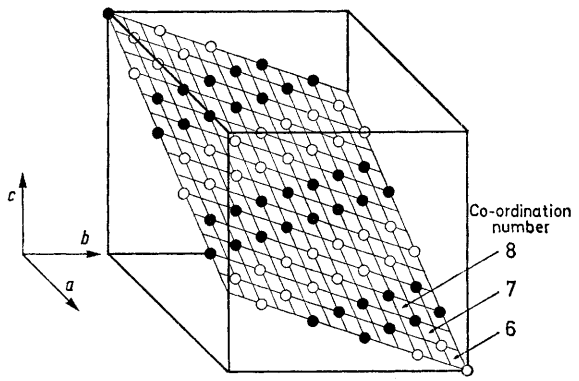

FIGURE 13 Location of vacant oxygen sites (○) on a (213) plane of $Zr_{10}Sc_4O_{26}$. Potential metal atom sites on [111] axis with co-ordination number = 6, 7, and 8 are marked [(●) indicates occupied oxygen site]

of the ι-Pr_7O_{12} phase. Disorder can be achieved by randomizing the sequence in which the rows are arranged.

(*ii*) An alternative procedure for disordering anion vacancies on a (213) plane is to randomly blend the requisite numbers of $Pr_{\frac{7}{2}}\square O_6$ and $Pr_{\frac{7}{2}}O_7$ units within each [$\bar{1}$20] row. Residual long-range order will be determined by the extent to which the resulting distribution of c.d.s is randomized. Effectively, both

the density and order of point defects contained in (213) planes can be diminished progressively by interchanging $Pr_{\frac{2}{3}}\square O_6$ and $Pr_{\frac{2}{7}}O_7$ until finally a purely statistical distribution over the plane remains. It is conceivable that this description would be appropriate for an α-phase at the higher temperatures where all but vestigial traces of longer-range order have disappeared. The residual order arises because the (213) planes remain regularly spaced at $7d/\sqrt{14}$ even though the distribution of defects over any plane is fully randomized.

Alternative Structural Models.—A feature of the topological analysis outlined above is the close packing of c.d.s to form linear progressions of vacant anion sites along [$\bar{1}\bar{1}\bar{1}$] axes [*cf.* Figures 6(*c*) and 9(*c*)]. The question arises whether this feature is unique or whether there are alternative arrangements of c.d.s which achieve the required close packing and preserve the cation sub-lattice intact for ordered phases.

A structure for β′-$Pr_{12}O_{22}$. It is interesting to speculate about the obvious stability of oxide phases in the region $x = 1{\cdot}83$ and whether alternative structures are permissible. Equilibria in Table 3 mostly conform to the idealized stoicheiometry (2), where β′ is believed [5]

$$mPr_nO_{2n-2} \rightleftharpoons \beta'\text{-}Pr_{12}O_{22} + (m-1)Pr_{(n-1)}O_{2n-4} \quad (2)$$

to be a disordered form of β-$Pr_{12}O_{22}$. Surprisingly, the β and β′ phases are immiscible although the diphasic region is extremely narrow with a maximum compositional width of $1{\cdot}827 < x < 1{\cdot}831$. However, it persists to extremely high pressures (*cf.* Table 3) which leads to the presumption of a radical and persistent structural difference between the two phases.

Topological considerations suggest that there is an alternative way of amalgamating five additional $Pr_{\frac{1}{3}}O$ octants with $Pr_{\frac{2}{3}}\square O_6$ to create a viable but crystallographically different structure for a phase of composition $Pr_{12}O_{22}$. Thus, if the lower row of close-packed c.d.s [*cf.* Figure 4(*a*)] is translated along the [$\bar{1}$30] direction through a distance *d*, a row of H cavities is created along the [$\bar{1}$20] direction. This procedure generates an (001) sheet of overall composition Pr_7O_{12} [Figure 14(*a*)]. A maximum of two such layers can be superimposed, the axial octants of one layer mating along the [$\bar{1}$20] directions with vacant holes H of the second layer. Both surfaces of the resulting ' duplex ' layer are left with axial octants projecting along [$\bar{1}$20] directions. If five $Pr_{\frac{1}{3}}O$ octants are now arranged to form a ' cross,' these $Pr_{\frac{2}{3}}O_5$ moieties can be arranged so as to generate a smooth (001) layer [Figure 14(*b*)] with the cavities again being disposed along [$\bar{1}$20] directions. When such layers of PrO_2 are superimposed on the surfaces of the ' duplex ' layer of Pr_7O_{12}, all the remaining axial octants are encapsulated. The resulting slab of overall composition $PrO_{1{\cdot}833}$ has a finite thickness of 4*d* with all the anion vacancies contained in contiguous pairs of (001) planes and ordered as shown in Figure 14(*a*).

[35] R. Collongues, M. Perez y Jorba, and J. LeFèvre, *Bull. Soc. chim.* (*France*), 1961, 70.

Although the composition is $Pr_{12}O_{22}$, the present structure differs fundamentally from that proposed for the β-homologue in Figures 8(*e*) and 9 and the observed immiscibility between them should be expected. In spite of this, both structure types possess topological characteristics which make them coherent with a fluorite PrO_2 matrix. Thus dispersion of the present β′ slabs in bulk PrO_2 could form an alternative basis for the disordered pseudo-cubic non-stoicheiometric f.c.c. α-phase in the region $1{\cdot}83 < x < 2{\cdot}00$. The β′ slabs need not be infinite and termination by coherent bulk

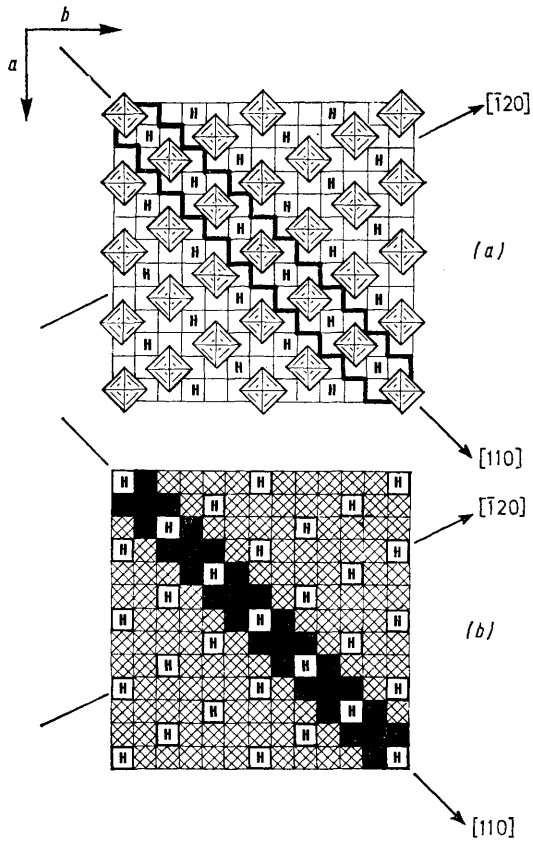

FIGURE 14 Conjectural structure for β′-$PrO_{1{\cdot}83}$: (*a*) layer of c.d.s with minimum number of mating holes H. (' Duplex ' row of c.d.s forms along the [110] directions.); (*b*) layer of $Pr_{\frac{1}{3}}O$ octants (cross-hatched) with correct topology to overlay the layer illustrated in (*a*) {Six characteristic $Pr_{\frac{2}{3}}O_5$ ' crosses ' along [110] direction are marked black. These exactly overlay [110] strand outlined in black in (*a*).}

PrO_2 could readily create finite discs comprised of the Pr_7O_{12} ' duplex ' layer. Unfortunately there is a dearth of information about phase relations in the region $1{\cdot}83 < x < 2{\cdot}0$ so that, at present, structural speculations of this nature cannot be evaluated.

The pyrochlore structure for M_8O_{14}. Evidence for the cubic pyrochlore structure, $E8_1$, is found in several ternary oxide systems such as ZrO_2–Gd_2O_3 and ZrO_2–La_2O_3, but is entirely absent in the corresponding ZrO_2–Nd_2O_3 and ZrO_2–Yb_2O_3 systems.[35,36] For the

[36] M. Perez y Jorba, R. Collongues, and J. LeFèvre, *Compt. rend.*, 1959, **249**, 1237.

composition $M_2^{III}M_2^{IV}O_7$ it is generally found that the larger M^{3+} cation lies at the centre of a deformed MO_8 cube (*cf.* the *C*1 structure) while the smaller M^{4+} cation is at the centre of a $MO_6\square_2$ cube where the missing anions lie along a body diagonal (as in the ι-M_7O_{12} structure). Clearly the $E8_1$ structure is closely related to fluorite and can be derived from it by ordered omission

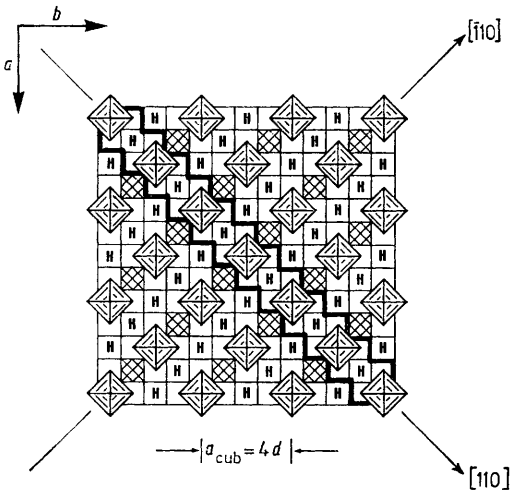

FIGURE 15 Arrangement of c.d.s in (001) layer of pyrochlore structure. Additional $Pr_{\frac{1}{2}}O$ octants are cross-hatched. Duplex rows of c.d.s form along [110] outlined in black

of 1/8 of the anions. Examination of the pyrochlore crystal structure [3,7] reveals that every anion vacancy is octahedrally co-ordinated by six nearest oxygen neighbours; *i.e.* the c.d. retains its integrity in this cubic structure. Association of one $M_{\frac{1}{2}}O$ octant with each $M_{\frac{2}{3}}\square O_6$ c.d. yields the M_8O_{14} composition which is the missing homologue in the praseodymium oxide + oxygen system.

The structure of a single (001) layer of pyrochlore is illustrated in Figure 15. Two such layers are stacked to give pairwise interactions between the c.d.s which are gathered along the [110] and [1̄10] directions, the second layer being first rotated through $\pi/2$ and then translated by d[111] with respect to the first layer. This procedure generates ' duplex ' rows of c.d.s along [110] which are identical to those proposed above for the β′-$Pr_{12}O_{22}$ phase. However, whereas adjoining ' duplex ' rows are contiguous in the proposed β′-structure [*cf.* Figure 14(*a*)], they are separated by rows of alternating $M_{\frac{1}{2}}O$ octants and H cavities along [110] in the pyrochlore phase (*cf.* Figure 15). The third and fourth layer of the unit cell of the $E8_1$ structure are likewise paired up to give ' duplex ' rows of c.d.s also along [110]. However, intermeshing of the two ' duplex ' layers at the interface of the second and third rows to give the crystallographic unit cell ($a_{cub.} = 4d$), although space filling, does not involve generation of a third ' duplex ' layer.

It is concluded that c.d.s can be close-packed in either of two ways to form infinite rows: (*i*) stacking along ⟨111⟩ to form congeneric Pr_nO_{2n-2} phases based on the ι-Pr_7O_{12} structure; and (*ii*) stacking along [110] to form ' duplex ' rows in which vacant anion sites are alternated by repeating d[111] and d[11$\bar{1}$] translations to yield an oscillating arrangement. The ' duplex ' row is then the extended defect on which the cubic pyrochlore, possibly β′-$Pr_{12}O_{22}$, and non-stoicheiometric α-PrO_x phases are based. These phases can be disordered as described earlier by progressive substitution of $Pr_{\frac{2}{3}}\square O_6$ by $Pr_{\frac{2}{3}}O_7$ units.

It can be speculated that the structural similarity between $E8_1$-Pr_8O_{14} and β′-$Pr_{12}O_{22}$ could account in part for the difficulty in obtaining evidence for the existence of this homologue. It is apparent from Table 3 that Pr_8O_{14} is bounded by the β′ and ι-Pr_7O_{12} phases, both of which possess considerable stability. If at the composition $x = 1{\cdot}75$ nuclei of the ' duplex ' row commence to form then it may well be that the energetics are delicately balanced and disproportionation according to equation (E) of Table 3 is thermodynamically favoured.

Conclusions.—In conclusion, it must be stressed that the structural hypothesis outlined above has been directed towards explaining long-range order which characterizes ordered Pr_nO_{2n-2} homologues and the residual texture of the non-stoicheiometric α-phase

TABLE 5

Relation between ordered Pr_nO_{2n-2} and disordered PrO_x phases assuming integrity of $M_{\frac{2}{3}}\square O_6$ is retained

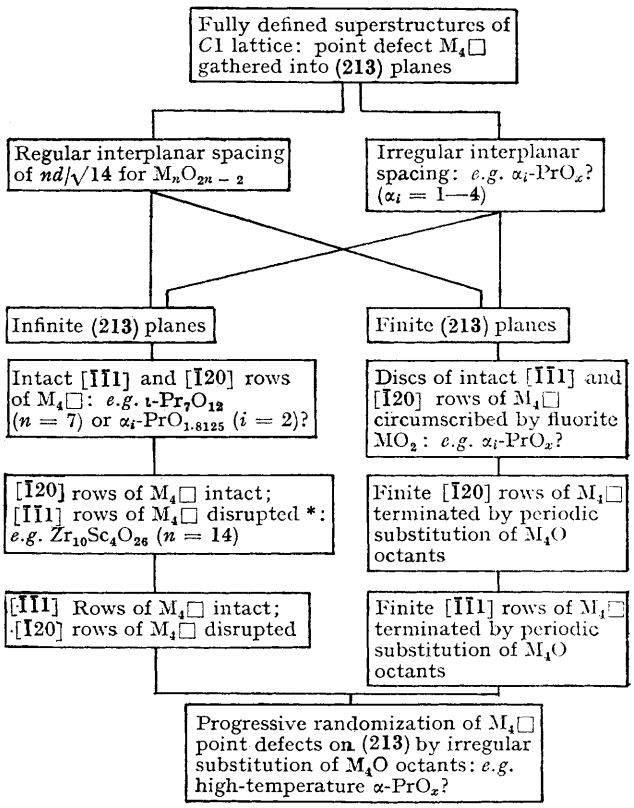

* Point defects assembled in $7/n$ of the n [1̄20] rows of Pr_nO_{2n-2} which lie on (213) planes spaced at $7d/\sqrt{14}$ (*cf.* Figure 13). Remaining $[1-(7/n)]$ of the n rows have been eliminated by replacing c.d.s by $Pr_{\frac{2}{3}}O_7$.

which envelopes their region of existence. Essentially, this long-range order is ascribed to packing characteristics of point defects whose topology in the fully co-ordinated condition is determined by strong short-range ordering forces.

The proposal that the co-ordination defect (c.d.) $M_{\frac{1}{2}}\square O_6$ is the fundamental entity which retains its integrity in ordered and disordered defect fluorite-type phases is reinforced by known crystal structures of the oxides $M_2O_3(D5_3)$, M_7O_{12}, $M_8O_{14}(E8_1)$, and $M_{14}O_{26}$. Topological analysis leads to the concept of planar ordering of defects in these materials but, unlike crystallographic shear in early transition-metal oxides, sheets of defects can be finite and terminated without distortion by replacing $M_{\frac{1}{2}}\square O_6$ with $M_{\frac{1}{2}}O_7$ units of identical topology. The progression from ordered stoicheiometric phases with fully defined superstructures to non-stoicheiometric phases with isolated random point defects can be summarized as in Table 5. The ordered pyrochlore M_8O_{14} and β'-$M_{12}O_{22}$ phases can likewise be disordered progressively by substituting $M_{\frac{1}{2}}O_7$ for $M_{\frac{1}{2}}\square O_6$.

It is suggested that the structural principles formulated in this article should be widely applicable to the defect solid state, especially to those compounds of ionic nature where forces of covalent character are largely absent. Once the stereochemistry of the basic c.d. is recognized, ordering of site vacancies in the appropriate sub-lattice derives primarily from its topological requirements. Topological analysis should then provide more detailed insight into the nature of the superstructures which accommodate deviations from stoicheiometry. These ideas will be extended in Part II of this series to suggest plausible structural relations for more-reduced lanthanoid oxides MO_x in the region $1{\cdot}5 < x < 1{\cdot}7$.

Added in proof: Although ι-Tb_7O_{12} is the only intermediate binary phase for which the structure is known,[6] the unit cell of β-$Pr_{12}O_{22}$ reported by Lowenstein *et al.*[38] has been confirmed recently in unpublished electron diffraction studies from superlattice patterns.[39] The volume found is six times that of the $C1$ unit cell ($8d^3$); illustrated in Figure 2(*b*). It is encouraging that the unit cell deduced here for the β-phase in Figures 8(*e*) and 9(*a*) has a volume of $48d^3$; *i.e.* six times that of the $C1$ unit cell.

I thank Professor J. S. Anderson, F.R.S., for constructive comments on the manuscript.

[3/2118 *Received*, 16*th October*, 1973]

[37] W. W. Barker, J. Graham, O. Knop, and F. Brisse, ' The Chemistry of Extended Defects in Non-metallic Solids,' eds. L. Eyring and M. O'Keeffe, North-Holland, Amsterdam, 1970, p. 198.

[38] M. Z. Lowenstein, L. Kihlborg, K. H. Lau, J. M. Haschke, and L. Eyring, *Proc. 5th Materials Research Symp.*, ' *Solid State Chemistry*,' NBS Spec. Publ. **364**, pp. 343—351.

[39] L. Eyring and L. Tai, *Ann. Rev. Phys. Chem.*, 1973, **24**, 189.